(17) S. R. Fletcher and A. C. Skapski, *J. Chem. Soc., Dalton Trans.*, 486 (1974).
(18) We take the van der Waals radii of sulfur and a cyclopentadienyl carbon atom to be 1.72–1.73 Å[19] and 1.7 Å,[20] respectively.
(19) D. van der Helm, A. E. Lessor, Jr., and L. L. Merritt, Jr., *Acta Crystallogr.*, **15**, 1227 (1962).
(20) L. Pauling, "The Nature of the Chemical Bond", 3rd ed, Cornell University Press, Ithaca, N.Y., 1960, p 260.
(21) N. F. M. Henry and K. Lonsdale, Ed., "International Tables for X-Ray Crystallography", Vol. 1, 3rd ed, The Kynoch Press, Birmingham, England, 1969, p 99.
(22) L. J. Radonovich, A. Bloom, and J. L. Hoard, *J. Am. Chem. Soc.*, **94**, 2073 (1972).
(23) D. T. Cromer and J. B. Mann, *Acta Crystallogr., Sect. A.*, **24**, 321 (1968).
(24) D. T. Cromer, *Acta Crystallogr., Sect. A*, **18**, 17 (1965).
(25) See paragraph at end of paper regarding supplementary material.
(26) E. L. Muetterties and L. J. Guggenberger, *J. Am. Chem. Soc.*, **96**, 1748 (1974). See also the erratum: E. L. Muetterties and L. J. Guggenberger, *ibid.*, **99**, 3893 (1977).
(27) Short S···S contacts in $Ru[S_2CN(C_2H_5)_2]_3Cl$,[12] $Mo(NO)[S_2CN(n\text{-}C_4H_9)_2]_3$,[16] and $Ti[SOCN(C_2H_5)_2]_4$[28] have been cited as evidence for attractive ligand interactions. However, it is more likely that the S···S interactions are repulsive[29] and that the easily deformed sulfur atoms can tolerate very short S···S distances.
(28) W. L. Steffen, S. L. Hawthorne, and R. C. Fay, *J. Am. Chem. Soc.*, **98**, 6757 (1976).
(29) W. L. Steffen and R. C. Fay, *Inorg. Chem.*, **17**, 2120 (1978).
(30) A. Kutoglu, *Z. Anorg. Allg. Chem.*, **390**, 195 (1972).
(31) A. Kutoglu, *Acta Crystallogr., Sect. B*, **29**, 2891 (1973).
(32) G. G. Aleksandrov and Yu. T. Struchkov, *J. Struct. Chem.*, **12**, 605 (1971).
(33) P. Corradini and A. Sirigu, *Inorg. Chem.*, **6**, 601 (1967).
(34) J. L. Calderon, F. A. Cotton, B. G. DeBoer, and J. Takats, *J. Am. Chem. Soc.*, **93**, 3592 (1971).
(35) E. F. Epstein and I. Bernal, *J. Organomet. Chem.*, **26**, 229 (1971).
(36) B. R. Davis and I. Bernal, *J. Organomet. Chem.*, **30**, 75 (1971).
(37) T. L. Khotsyanova and S. I. Kuznetsov, *J. Organomet. Chem.*, **57**, 155 (1973).
(38) A. C. Villa, A. G. Manfredotti, and C. Guastini, *Acta Crystallogr., Sect. B*, **32**, 909 (1976).
(39) V. V. Tkachev and L. O. Atovmyan, *J. Struct. Chem.*, **13**, 263 (1972).
(40) V. Kocman, J. C. Rucklidge, R. J. O'Brien, and W. Santo, *Chem. Commun.*, 1340 (1971).
(41) S. J. Anderson, D. S. Brown, and A. H. Norbury, *J. Chem. Soc., Chem. Commun.*, 996 (1974).
(42) P. J. Wheatley, *Perspect. Struct. Chem.*, **1**, 9 (1967).
(43) (a) D. Coucouvanis, *Prog. Inorg. Chem.*, **11**, 223 (1970); (b) R. Eisenberg, *ibid.*, **12**, 295 (1970).
(44) S. Merlino, *Acta Crystallogr., Sect. B*, **24**, 1441 (1968), and references cited therein.
(45) P. W. G. Newman, C. L. Raston, and A. H. White, *J. Chem. Soc., Dalton Trans.*, 1332 (1973).
(46) P. W. G. Newman and A. H. White, *J. Chem. Soc., Dalton Trans.*, 2239 (1972).
(47) J. G. M. van der Aalsvoort and P. T. Beurskens, *Cryst. Struct. Commun.*, **3**, 653 (1974).
(48) C. S. Harreld and E. O. Schlemper, *Acta Crystallogr., Sect. B*, **27**, 1964 (1971).
(49) A. Kopwillem, *Acta Chem. Scand.*, **26**, 2941 (1972).
(50) L. Ricard, C. Martin, R. Wiest, and R. Weiss, *Inorg. Chem.*, **14**, 2300 (1975).
(51) J. G. Leipoldt and P. Coppens, *Inorg. Chem.*, **12**, 2269 (1973).
(52) H. Abrahamson, J. R. Heiman, and L. H. Pignolet, *Inorg. Chem.*, **14**, 2070 (1975).
(53) M. Ciampolini, C. Mengozzi, and P. Orioli, *J. Chem. Soc., Dalton Trans.*, 2051 (1975).
(54) P. C. Healy and A. H. White, *J. Chem. Soc., Dalton Trans.*, 284 (1973).
(55) P. C. Healy and A. H. White, *J. Chem. Soc., Dalton Trans.*, 1883 (1972).
(56) P. C. Healy, A. H. White, and B. F. Hoskins, *J. Chem. Soc., Dalton Trans.*, 1369 (1972).
(57) L. H. Pignolet, *Inorg. Chem.*, **13**, 2051 (1974).
(58) D. F. Lewis and R. C. Fay, *Inorg. Chem.*, **15**, 2219 (1976).
(59) B. P. Stoicheff, *Can. J. Phys.*, **32**, 339 (1954).
(60) E. G. Cox, D. W. J. Cruickshank, and J. A. S. Smith, *Proc. R. Soc. London, Sec. A*, **247**, 1 (1958).

Contribution from the Laboratoire de Chimie de Coordination du CNRS, 31030 Toulouse, France, and the Institut de Chimie Minérale et Analytique, Université de Lausanne, 1005 Lausanne, Switzerland

Stereochemically Nonrigid Pentacoordinate Nickel(II) Complexes. X-ray Structure of Bromotetrakis(trimethylphosphine)nickel(II) Tetrafluoroborate and Solution Study of $[NiX(PMe_3)_4]BF_4$ (X = Cl, Br, I)[1]

M. DARTIGUENAVE,*[2a] Y. DARTIGUENAVE,[2a] A. GLEIZES,[2a] C. SAINT-JOLY,[2a] J. GALY,[2a] P. MEIER,[2b] and A. E. MERBACH[2b]

Received July 19, 1978

New cationic Ni(II) complexes $[NiX(PMe_3)_4]BF_4$ have been isolated and studied thoroughly in the solid state and in dichloromethane solution, using the X-ray diffraction technique, variable-temperature electronic spectroscopy, and $^{31}P\{^1H\}$ Fourier mode NMR. The crystal and molecular structure of bromotetrakis(trimethylphosphine)nickel(II) tetrafluoroborate has been determined from the three-dimensional X-ray data collected by counter methods. Full-matrix least-squares refinement of the structure has led to a final conventional R factor on F of 0.072. The crystals have orthorhombic symmetry, space group *Pbca*, with eight molecules per unit cell of dimensions a = 16.029 (4) Å, b = 25.179 (4) Å, and c = 11.413 (2) Å. The crystallographically derived density is 1.527 g cm^{-3}. The crystal chemical unit consists of separate cationic $[NiX(PMe_3)_4]^+$ and anionic BF_4^- entities. The geometry around the Ni atom is a somewhat distorted version of a trigonal bipyramid of C_{2v} symmetry with the bromine atom in an equatorial position. The two axial Ni–P bond distances are 2.247 (4) and 2.244 (4) Å while the slightly longer equatorial Ni–P lengths are 2.257 (5) and 2.290 (5) Å. The Ni–Br bond distance is 2.515 (2) Å and the P_{ax}–Ni–P_{ax} bond angle is 167.1 (2) Å. Solid-state and solution electronic spectra of $[NiX(PMe_3)_4]BF_4$ (X = Cl, Br, I) have been measured at 295, 180, and 77 K and the results compared to those of the variable-temperature $^{31}P\{^1H\}$ Fourier mode NMR spectra. The three complexes have the C_{2v} structure in the solid state and in solution, at room and low temperature, provided an excess of PMe_3 is present to prevent dissociation. They are stereochemically nonrigid at 295 K on the NMR time scale. Phosphorus exchange has been shown to occur through an intramolecular rearrangement following the Berry pseudorotation process. The rate of this rearrangement is in the order $k_{Cl} > k_{Br} > k_I$. The measured free energies of activation are $\Delta G^* = 6.6 \pm 0.2$ (Cl), 7.8 ± 0.2 (Br), and 8.2 ± 0.2 (I) kcal mol^{-1} at 169 K.

I. Introduction

Although the existence of low-spin molecular NiX_2L_3 and cationic $[NiL_5]^{2+}$ complexes is now well established with monodentate phosphine, phosphite, arsine, and stibine ligands,[3,4] only few cationic $[NiXL_4]^+$ complexes have been reported: $[NiH(PMe_3)_4]^+$,[5] $[Ni(CH_3)(PMe_3)_4]^+$,[6] $[NiX(PHEt)_4]^+$,[7] $[NiBr(P(OMe)_3)_4]^+$.[8]

Recently,[9] we have communicated the first NMR evidence that when X = halide, the pentacoordinate NiX_2L_3 and $(NiXL_4)X$ species are closely related in dichloromethane solution by the equilibrium

$$NiX_2(PMe_3)_3 + PMe_3 \underset{295\ K}{\overset{180\ K}{\rightleftharpoons}} [NiX(PMe_3)_4]^+X^- \quad (1)$$

As a continuing part of this investigation, initiated to obtain quantitative information on how different factors (nature of X and L, solvent, temperature) influenced the existence and the stereochemistry of each species, we have prepared the

0020-1669/78/1317-3503$01.00/0

$[NiX(PMe_3)_4]^+$ complexes as tetrafluoroborate salts (X = Cl, Br, I). The crystal and molecular structure of $[NiBr(PMe_3)_4]BF_4$ has been determined. The solution structure has been characterized for the three halides by variable-temperature electronic and NMR spectroscopy. We report NMR evidence for stereochemical rigidity in a C_{2v} $[MXL_4]^+$ complex, where a Berry process may operate, a result of interest since previous investigations have indicated that for molecules of this symmetry, the barriers to intramolecular rearrangement are low, usually smaller than 10 kcal/mol.[10] Stereochemical rigidity was obtained for $[Ni(CH_3)(PMe_3)_4]^+$ by Klein and Karsch[6] and for $[NiH(PEt_3)_4]^+$ (at −150 °C) by English, Meakin, and Jesson,[5] but this was expected since the complexes present a trigonal-bipyramidal geometry with CH_3 and H in axial position (C_{3v}).

Prior to this work, similar equilibria in Ni(II) chemistry had been established by Rigo and Bressan[7] with diethylphosphine, $PHEt_2$, by electronic spectroscopy, but no definitive conclusions on the stereochemistry of the complexes had been drawn.

II. Experimental Section

Preparation. Trimethylphosphine was prepared by the method of Wolfsberger and Schmidbaur[11] and stored under argon in a tightly stoppered ampule. All metal salts were reagent grade (Alfa) and were used without further purification. Dichloromethane (Fluka) was dried and redistilled from $CaCl_2$ and then stored on molecular sieves. Absolute ethanol was dried by distillation over Mg at 77–78 °C. All of the preparative work was carried out under an atmosphere of dry argon to prevent oxidation of the trimethylphosphine. The solvents were degassed prior to use. Since all of the syntheses followed the same procedure, only the preparation of $[NiBr(PMe_3)_4]BF_4$ is presented in detail.

Bromotetrakis(trimethylphosphine)nickel(II) Tetrafluoroborate, $[NiBr(PMe_3)_4]BF_4$. A 2.4-mL (25-mmol) sample of PMe_3 was added dropwise to a solution of $NiBr_2 \cdot 3H_2O$ (0.68 g, 2.5 mmol) and $Ni(BF_4)_2 \cdot 6H_2O$ (0.85 g, 2.5 mmol) in absolute ethanol (20 mL) in the presence of 2,2-dimethoxypropane (5 mL) at −70 °C. Dark violet microcrystals which separate immediately were collected on a frit and washed with ethanol. They were soluble in dichloromethane and in acetone. By recrystallization in a mixture of CH_2Cl_2–EtOH (1:1), with a slight excess of PMe_3, violet-blue crystals are obtained at room temperature (yield 95%).

Physical Measurements. Electronic spectra were measured on a Cary 14 spectrophotometer using deoxygenated CH_2Cl_2 solutions (concentration of complex 10^{-2} M) in 0.100-cm silica cells. The cells were held in a variable-temperature Oxford DN 702 Dewar. The solid-state spectra were examined by using Nujol as a support. Gaussian analyses were performed on the spectra by using a du Pont Model 310 curve resolver.

Magnetic susceptibilities were determined by the Faraday method, using a Cahn microbalance coupled with a Drusch electromagnet. Experimental values are the mean of three determinations at 295 K. They are corrected for the diamagnetism of the ligands.[12]

Conductivities of 10^{-3} M solutions (with excess PMe_3) were measured using a Beckman RC-18 conductivity bridge.

Variable-temperature proton noise-decoupled Fourier mode ^{31}P NMR spectra were recorded in 10-mm sealed sample tubes at 24.28 MHz using a Brucker WP-60 spectrometer equipped with a proton noise decoupler, a frequency synthesizer, and a broad-band pulse power amplifier and cascade. The temperature was regulated with a Brucker B-ST 100/700 temperature unit and measured by a method described elsewhere.[13] Field frequency stabilization was achieved on an external ^{19}F signal. The complexes (10^{-2} M) were weighed in a drybox (KSE) directly into the NMR sample tubes. The solvents ($CHClF_2$ or CH_2Cl_2) were deoxygenated in an all-glass–Teflon vacuum line by the freeze–pump–thaw technique and vacuum distilled onto the solid samples. PMe_3 (10^{-2} M/L) was added by the same method. The tubes were sealed under vacuum and stored in liquid nitrogen. As a ^{31}P chemical shift reference we used pure PEt_3 in a capillary. Since the chemical shift of PEt_3 is temperature dependent (about 0.027 ppm/K), we measured the chemical shift difference between PEt_3 and 62.5% H_3PO_4 (eutectic) as a function of temperature. All chemical shifts are reported with respect to 62.5% H_3PO_4, with downfield shifts considered positive. The intramolecular phosphine exchange rates were determined at one temperature by visual comparison of experimental and calculated spectra. The computer program used was PZDMCS kindly supplied by P. Meakin. The exchange vector used implies simultaneous exchange of the two axial phosphines with the two equatorial ones in the $[NiX(PMe_3)_4]BF_4$ molecule. The temperature dependence of the ^{31}P chemical shifts have been taken into account when necessary.

Elemental microanalyses were performed by the Service de Microanalyse du CNRS in Montpellier, France.

Table I

(1) Physical and Crystallographic Data

formula: $[NiBr(PMe_3)_4]^+BF_4^-$	$V = 4606$ Å^3
crystal system: orthorhombic	$Z = 8$
$a = 16.029$ (4) Å	$F(000) = 2176$
$b = 25.179$ (4) Å	absorption factor: $\mu_{Mo\ K\alpha} = 28.7$ cm^{-1}
$c = 11.413$ (2) Å	morphology: cylinder along ($h00$); $\phi = 0.051$ cm (diameter); $L = 0.046$ cm (length)
ρ_{expd} was not measd	
$\rho_x = 1.527$ g/cm^3	
mol wt: 529.74	
space group: *Pbca*	

(2) Data Collection

temp: 297 K
radiation: λ(Mo Kα) = 0.710 69 Å
crystal–detector distance: 208 mm
detector window: height (mm) = 4; width (mm) = 2.6 + 1.90 tan θ
takeoff angle: 2.7°
scan mode: θ–2θ
maximum Bragg angle: 28°
scan angle: $\Delta\theta = \Delta\theta_0 + B \tan\theta$, $\Delta\theta_0{}^a = 0.70°$, $B^a = 0.347°$
value determinating the scan speed: SIGPRE[a] = 0.330, SIGMA[a] = 0.018, VPRE[a] = 20°/min, TMAX[a] = 90
test reflections: 600, $\overline{8}60$, 486 (intensity); 0,24,0, 0,12,5, $\overline{4}86$ (orientation)
periodicity 3600 s, 100 reflections

[a] These parameters have been described in A. Mosset, J.-J. Bonnet, and J. Galy, *Acta Crystallogr., Sect. B*, **33**, 2639 (1977).

X-ray Data Collection. A single crystal suitable for X-ray analysis was sealed into a Lindemann glass capillary. Preliminary precession photographs indicating Laue symmetry *mmm* and systematic absences $0kl$, $k = 2n + 1$, $h0l$, $l = 2n + 1$, and $hk0$, $k = 2n + 1$ were consistent with space group $D_{2h}{}^{15}$-*Pbca*.

Then the crystal was mounted on an Enraf–Nonius CAD 4 computer-controlled four-circle diffractometer. The unit cell constants were derived from a least-squares refinement of the setting angles of 25 reflections. Reflections with positive or null indices were collected up to a Bragg angle $\theta = 28°$ using graphite-monochromatized Mo Kα radiation. Physical and crystallographic data along with data collection conditions are listed in Table I.

Peak counts were corrected from background to yield net integrated intensities I which were assigned standard deviations calculated according the formula

$$\sigma(I) = [CT + 0.25(t_c/t_b)^2(B_1 + B_2) + (pI)^2]^{1/2}$$

CT is the total integrated peak count obtained during a scan time t_c, B_1 and B_2 are background counts obtained during a scan time t_b, and $I = CT - 0.5(t_c/t_b)(B_1 + B_2)$. The value of p was selected as 0.02. Then, intensities were rescaled over an overall decrease by 5% of the three standard reflections intensities and then corrected for Lorentz and polarization effects. No absorption corrections were made since the relatively low absorption coefficient value $\mu = 28.7$ cm^{-1}, combined with the smallness and the relatively isotropical shape of the crystal, yields nearly isotropical $\overline{\mu R} = 0.7$.

Among the 5001 reflections collected, 4458 were independent reflections of which, after elimination of systematic absences, 1867 had $I > 2\sigma(I)$ and were used in subsequent refinement of the structure parameters.

Structure Solution and Refinement. Refinement of the structure was effected by full-matrix least-squares techniques.[14] Throughout the refinement, the function minimized was $\sum w(|F_o| - |F_c|)^2$, where $|F_o|$ and $|F_c|$ are the observed and calculated structure amplitudes and the weight w is $4F_o{}^2/\sigma^2(F_o)^2$. The atomic scattering factors for all

Table II. Final Positional and Thermal Parameters for $[NiBr(PMe_3)_4]BF_4$[a]

atom	x	y	z	B_{11}	B_{22}	B_{33}	B_{12}	B_{13}	B_{23}
Ni	0.08074 (10)	0.10373 (6)	0.25098 (19)	2.20 (8)	0.99 (3)	4.40 (15)	−0.06 (5)	0.01 (13)	0.13 (9)
Br	0.06049 (10)	0.93509 (7)	0.70579 (16)	2.40 (7)	1.73 (3)	11.73 (20)	−0.34 (5)	0.47 (11)	0.88 (8)
P(1)	0.01097 (24)	0.18112 (15)	0.2515 (5)	2.50 (18)	1.16 (7)	6.3 (4)	0.19 (9)	−0.05 (29)	−0.12 (20)
P(2)	0.12157 (22)	0.01850 (15)	0.2510 (5)	2.55 (17)	0.99 (7)	6.1 (4)	−0.13 (10)	−0.4 (3)	0.55 (22)
P(3)	0.15095 (29)	0.12313 (19)	0.4204 (4)	3.10 (24)	1.49 (13)	3.7 (4)	−0.17 (14)	−0.37 (27)	0.01 (18)
P(4)	0.13520 (28)	0.11990 (19)	0.0721 (4)	2.91 (23)	1.13 (11)	5.0 (5)	−0.11 (13)	0.11 (26)	0.29 (18)
C(11)	0.0658 (9)	0.2438 (5)	0.2169 (12)	5.0 (8)	1.12 (28)	7.0 (18)	−0.4 (5)	0.0 (11)	0.5 (6)
C(21)	0.0785 (9)	0.8174 (6)	0.8496 (13)	2.6 (8)	1.7 (4)	6.2 (17)	0.1 (5)	−2.0 (10)	0.3 (6)
C(31)	0.0374 (9)	0.8016 (6)	0.6081 (13)	2.5 (8)	1.8 (4)	5.3 (17)	0.5 (5)	1.6 (9)	−0.8 (6)
C(12)	0.9364 (11)	0.0222 (6)	0.8517 (13)	6.0 (10)	0.8 (3)	8.2 (18)	−0.8 (6)	−1.3 (12)	−1.2 (6)
C(22)	0.7665 (8)	0.9990 (5)	0.7770 (12)	1.3 (6)	1.5 (3)	4.9 (18)	0.3 (4)	−0.1 (9)	0.4 (6)
C(32)	0.8984 (9)	0.0164 (6)	0.6118 (13)	3.6 (9)	1.2 (3)	6.2 (17)	−0.5 (5)	0.4 (10)	1.6 (6)
C(13)	0.8131 (9)	0.8091 (6)	0.5570 (15)	3.0 (8)	0.6 (3)	10.0 (21)	−0.5 (5)	−0.8 (10)	−0.9 (7)
C(23)	0.7490 (9)	0.9121 (6)	0.5526 (13)	2.3 (7)	1.2 (3)	7.1 (17)	0.7 (4)	−1.9 (10)	0.3 (6)
C(33)	0.9065 (11)	0.8907 (7)	0.4424 (12)	5.7 (10)	3.3 (5)	2.5 (14)	−1.6 (6)	3.1 (10)	0.1 (7)
C(14)	0.8293 (11)	0.9340 (7)	0.0310 (13)	7.1 (11)	1.9 (4)	5.2 (17)	1.4 (6)	1.7 (11)	−0.5 (7)
C(24)	0.9195 (10)	0.8385 (6)	0.0382 (13)	5.4 (11)	1.8 (4)	4.3 (16)	0.9 (6)	−1.3 (11)	0.9 (6)
C(34)	0.7659 (10)	0.8427 (7)	0.9066 (15)	3.8 (10)	1.9 (4)	10.0 (21)	−1.5 (5)	1.5 (12)	0.3 (8)
B	0.1716 (18)	0.8296 (9)	0.251 (4)	7.9 (16)	1.6 (4)	7.8 (24)	−0.1 (8)	−2.2 (26)	1.4 (17)
F(1)	0.2256 (8)	0.8684 (5)	0.2506 (15)	13.3 (11)	3.5 (3)	23.5 (19)	−4.2 (5)	0.7 (16)	−1.8 (9)
F(2)	0.1282 (10)	0.8293 (7)	0.1511 (13)	12.7 (12)	7.0 (6)	12.1 (19)	−1.7 (7)	−4.9 (12)	0.2 (8)
F(3)	0.1246 (10)	0.8278 (7)	0.3443 (14)	13.7 (13)	7.1 (7)	15.7 (21)	−1.1 (7)	8.9 (14)	−0.6 (9)
F(4)	0.2144 (9)	0.7828 (5)	0.2452 (19)	13.1 (12)	3.9 (3)	38.0 (29)	2.0 (6)	1.8 (19)	2.9 (12)

[a] Estimated standard deviations in the least significant figure(s) are given in parentheses in this and all subsequent tables. The form of the anisotropic thermal ellipsoid is $\exp[-(B_{11}h^2 + B_{22}k^2 + B_{33}l^2 + 2B_{12}hk + 2B_{13}hl + 2B_{23}kl)]$. The quantities given in the table are the thermal coefficients $\times 10^3$.

Table IV. Root-Mean-Square Amplitudes of Vibration (A) of Atoms in $[NiBr(P(CH_3)_3)_4]BF_4$

atom	min	inter	max
Ni	0.166 (7)	0.169 (10)	0.182 (4)
Br	0.168 (3)	0.230 (3)	0.289 (3)
P(1)	0.174 (7)	0.196 (7)	0.206 (7)
P(2)	0.164 (10)	0.178 (7)	0.216 (8)
P(3)	0.154 (10)	0.199 (8)	0.222 (9)
P(4)	0.171 (9)	0.194 (9)	0.200 (9)
C(11)	0.18 (3)	0.22 (3)	0.26 (2)
C(21)	0.14 (4)	0.23 (3)	0.24 (3)
C(31)	0.12 (4)	0.22 (3)	0.25 (3)
C(12)	0.11 (5)	0.25 (3)	0.29 (3)
C(22)	0.12 (3)	0.18 (3)	0.22 (2)
C(32)	0.11 (4)	0.22 (3)	0.26 (3)
C(13)	0.10 (4)	0.21 (3)	0.27 (3)
C(23)	0.11 (4)	0.21 (3)	0.24 (3)
C(33)	0.05 (8)	0.26 (3)	0.36 (3)
C(14)	0.15 (4)	0.23 (3)	0.33 (3)
C(24)	0.13 (4)	0.24 (3)	0.29 (3)
C(34)	0.14 (4)	0.26 (3)	0.29 (3)
B	0.17 (7)	0.26 (5)	0.33 (4)
F(1)	0.22 (2)	0.39 (2)	0.49 (2)
F(2)	0.24 (2)	0.41 (2)	0.49 (2)
F(3)	0.23 (2)	0.45 (2)	0.50 (2)
F(4)	0.31 (2)	0.42 (2)	0.52 (2)

atoms and the anomalous terms for nickel, bromine, phosphorus, and fluorine atoms are obtained from the tabulation in ref 15. The agreement indices R and R_w are defined as

$$R = \sum(||F_o| - |F_c||)/\sum F_o$$

$$R_w = (\sum w(|F_o| - |F_c|)^2/\sum wF_o^2)^{1/2}$$

An E map resulting from a direct method using the MULTAN program[14] clearly revealed the positions of the nickel, bromine, and four phosphorus atoms. Refinement of these coordinates with isotropic temperature factors gave $R = 0.22$ and $R_w = 0.31$. On subsequent Fourier and difference Fourier syntheses, all other atoms but hydrogen were found. Refinement of all nonhydrogen atoms using isotropic temperature factors resulted in $R = 0.088$ and $R_w = 0.090$. Next, anisotropic temperature factors were introduced yielding $R = 0.072$ and $R_w = 0.068$. A secondary extinction effect was found to be weakest through the refinement of Zachariasen's parameter. Convergence was achieved with $R = 0.072$ and $R_w = 0.066$ for the 1867 reflections and 209 variables. In the last cycle of refinement, variable shifts were less than 1% of their standard deviations for nickel, bromine, phosphorus, and carbon atoms and less than 4% for boron and fluorine atoms. The error in an observation of unit weight was 2.0 electrons. On a final difference Fourier map, the maximum remaining electron density did not exceed one-sixth of the value corresponding to a boron atom on a Fourier map. Hydrogen atoms could not be located. Refined atomic parameters are listed in Table II. Values of observed and calculated structure amplitudes are given in Table III and are available as supplementary material. Derived root-mean-square amplitudes of vibration for the atoms are listed in Table IV.

III. Results

The physical properties of the complexes are listed in Table V. The extinction coefficients and the positions of the ligand field transitions are given in Table VI. The $^{31}P\{^1H\}$ NMR data—chemical shifts and phosphorus–phosphorus coupling constants—are reported in Table VII.

The complexes $[NiX(PMe_3)_4]BF_4$ are blue-violet when crystallized at room temperature. They are reasonably stable in the solid state and can be handled in air. They are soluble in dichloromethane, acetone, and water but insoluble in ethanol and benzene. However, the room-temperature dichloromethane solutions are not stable and must be kept in an inert atmosphere, and an excess of PMe_3 is necessary to prevent decomposition of the pentacoordinate species. Fresh solutions behave as 1:1 electrolytes in CH_2Cl_2, in the presence of excess PMe_3.

Table V. General Physical Data and Analysis of $[NiX(PMe_3)_4]BF_4$ Complexes

compd	color	Λ,[a] Ω^{-1} mol^{-1} cm^2	μ_{eff}, μ_B	%C calcd	%C found	%H calcd	%H found
$[NiCl(PMe_3)_4]BF_4$	violet-blue	25.3	0.48[b]	29.70	29.47	7.48	7.42
$[NiBr(PMe_3)_4]BF_4$	violet-blue	22.3	0.81[b]	27.19	27.13	6.80	6.81
$[NiI(PMe_3)_4]BF_4$	violet-blue	20.2	0.91[c]	24.99	24.32	6.29	6.08

[a] 10^{-3} M in CH_2Cl_2 (PMe_3 total/Ni = 14); reference $(NBu_4)Cl = 19.12\ \Omega^{-1}$ mol^{-1} cm^2. [b] 295 K crystals. [c] Unrecrystallized compounds.

Table VI. Solution and Solid-State Electronic Spectra of the $[NiX(PMe_3)_4]BF_4$ Complexes $\nu \times 10^{-3}$ cm^{-1} $(\epsilon)^a$

compd	Nujol mull		CH_2Cl_2 solutions							
			$PMe_3/Ni = 4$		$PMe_3/Ni = 5$		$PMe_3/Ni = 14$			
	295 K	77 K	295 K	180 K	295 K	180 K	295 K		180 K	
$[NiCl(PMe_3)_4]BF_4$	16.7	16.7		16.3[b] (390)	15.0[b] (460)	16.6[b] (670)	15.3[b] (700)		16.0[b] (450)	
	c	18.9	18.3[c] (1060)	18.8[b] (1500)	17.9[b] (1600)	18.9[b] (2260)	18.0[b] (1800)	17.4 (1900)	18.58[b] (2400)	18.5 (2500)
		26.3		19.0 (1600)	17.7 (1780)	18.9 (2400)				
				26.0 (200)		26.0 (670)				
$[NiBr(PMe_3)_4]BF_4$	16.1	16.4		14.6[d]	16.0[b] (450)		16.2[b] (460)			
	18.2	18.4	18.5[c] (1190)	18.7 (1960)	18.4[b] (1660)	18.7 (2900)	18.3[b] (1630)	18.2 (1760)	18.7 (2600)	
	25.6	26.3				26.3 (390)			26.3 (300)	
$[NiI(PMe_3)_4]BF_4$			13.7 (360)[d]	13.7 (640)[d]						
	17.5	18.2	17.2 (1300)	17.8 (1600)	18.1 (3000)	18.3 (3300)		17.7 (2550)	18.3 (4000)	
		23.8		25.6 (1000)						
			28.1 (2900)	29.4 (2750)	29.0 (1600)	29.5 (1800)				

[a] The values are not corrected from the solvent contraction between 295 and 180 K. [b] Gaussian analysis. [c] Broad (no justifiable Gaussian analysis can be performed). [d] Ligand field transitions of the molecular $NiX_2(PMe_3)_3$ species.

Table VII. $^{31}P\{^1H\}$ NMR Data

species	δ $(PMe_3)^{a,d}$ axial	δ $(PMe_3)^{a,d}$ equat	J_{PP}[b]	T[c]	solvent
$[NiCl(PMe_3)_4]^+$	broad resonance			163	CH_2Cl_2
	+1.0 (t)	−28.8 (t)	82.5	115	$CHClF_2$
$[NiBr(PMe_3)_4]^+$	−2.6 (t)	−29.2 (t)	79.0	163	CH_2Cl_2
	−1.8 (t)	−27.8 (t)	80.5	115	$CHClF_2$
$[NiI(PMe_3)_4]^+$	−5.2 (t)	−29.2 (t)	76.5	163	CH_2Cl_2
	−5.0 (t)	−28.8 (t)	75.5	115	$CHClF_2$
$NiCl_2(PMe_3)_3$	−0.3 (d)	−35.0 (t)	78.7	165	CH_2Cl_2
$NiBr_2(PMe_3)_3$	−3.7 (d)	−30.4 (t)	71.6	165	CH_2Cl_2
$NiI_2(PMe_3)_3$	−8.6 (d)	−28.0 (t)	59.8	165	CH_2Cl_2
$[Ni(PMe_3)_5]^{2+}$	+0.9 (q)	−32.7 (t)	70.6	113	$CHClF_2$

[a] In ppm (positive shift downfield from 62.5% H_3PO_4), free PMe_3 = −61.2 ppm. [b] In hertz. [c] In kelvin. [d] d = doublet, t = triplet, q = quartet.

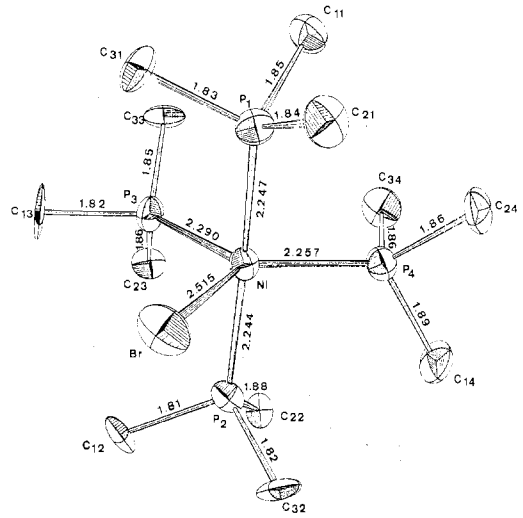

Figure 1. Perspective drawing of the $[NiBr(PMe_3)_4]^+$ cation.

All of the solid compounds are low spin, with room-temperature μ_{eff} values corresponding to a singlet ground state. However, the μ_{eff} values of 0.48 μ_B (X = Cl), 0.81 μ_B (X = Br), and 0.91 μ_B (X = I) are somewhat high for diamagnetic complexes but still in the range of the values reported for this class of Ni(II) complexes.[4]

A. Solid-State Study. A.1. Description of the X-ray Structure of $[NiBr(PMe_3)_4]BF_4$. The X-ray-derived main bonding and nonbonding distances and angles for a blue-violet $[NiBr(PMe_3)_4]BF_4$ crystal are shown in Table VIII. The unit cell contains eight cationic entities $[NiBr(PMe_3)_4]^+$ and eight anionic entities BF_4^-. The methyl–fluorine closest contact of 3.36 (2) Å does not differ significantly from the sum of the van der Waals radii[16] (3.35 Å) of a methyl group (2.0 Å) and a fluorine atom (1.35 Å), suggesting only weak anion–cation interactions.

The geometry of $[NiBr(PMe_3)_4]^+$ along with selected bond lengths and the numbering system of atoms is presented in Figure 1. The inner coordination sphere around the nickel atom is a somewhat distorted trigonal bipyramid with bromine and phosphorus P(3) and P(4) atoms occupying the equatorial positions. The geometry of nickel environment in $[NiBr(PMe_3)_4]^+$ is remarkably similar to the one previously described for $[NiBr(P(OMe)_3)_4]^+$ by Verkade et al.[8] In order to facilitate comparison, the values of nickel–ligand bond lengths, ligand–ligand distances, and angles around the nickel atom in the phosphite species are reported in parentheses after the corresponding values for the phosphine species in Table VII. Since both cation geometries have been derived from solid-state structures including BF_4^- as the counterion, the observed discrepancies between equivalent values mainly reflect the different steric sizes of phosphine and phosphite ligands.

Table VIII. Intramolecular Main Bond and Nonbonded Distances (Å) and Angles (deg) in $[NiBr(PMe_3)_4]BF_4$

Distances around Ni					
Ni-P(1)	2.247 (4)	(2.181 (2))[a]	Ni-P(4)	2.257 (5)	(2.187 (2))
Ni-P(2)	2.244 (4)	(2.180 (2))	Ni-Br	2.515 (2)	(2.456 (1))
Ni-P(3)	2.290 (5)	(2.239 (2))			
Angles around Ni					
P(1)-Ni-P(2)	167.1 (2)	(172.26 (10))	P(2)-Ni-P(4)	93.4 (2)	(91.98 (8))
P(1)-Ni-P(3)	93.3 (2)	(90.40 (8))	P(2)-Ni-Br	83.7 (2)	(85.50 (6))
P(1)-Ni-P(4)	92.2 (2)	(92.10 (8))	P(3)-Ni-P(4)	122.4 (2)	(124.31 (9))
P(1)-Ni-Br	83.6 (1)	(86.76 (7))	P(3)-Ni-Br	111.1 (1)	(112.24 (7))
P(2)-Ni-P(3)	93.5 (2)	(92.73 (8))	P(4)-Ni-Br	126.6 (2)	(123.44 (7))
Ligand-Ligand Distances					
P(1)-P(2)	4.462 (5)	(4.351 (2))[a]	P(2)-P(4)	3.277 (6)	(3.141 (2))
P(1)-P(3)	3.299 (7)	(3.137 (3))	P(2)-Br	3.182 (4)	(3.154 (2))
P(1)-P(4)	3.246 (7)	(3.145 (3))	P(3)-P(4)	3.984 (5)	(3.914 (2))
P(1)-Br	3.180 (4)	(3.192 (2))	P(3)-Br	3.964 (5)	(3.900 (2))
P(2)-P(3)	3.301 (6)	(3.198 (2))	P(4)-Br	4.264 (5)	(4.091 (2))
Distances around P Atoms					
P(1)-C(11)	1.85 (1)	P(2)-C(22)	1.88 (1)	P(3)-C(33)	1.85 (1)
P(1)-C(21)	1.84 (1)	P(2)-C(32)	1.82 (1)	P(4)-C(14)	1.89 (1)
P(1)-C(31)	1.83 (1)	P(3)-C(13)	1.82 (1)	P(4)-C(24)	1.86 (1)
P(2)-C(12)	1.81 (1)	P(3)-C(23)	1.86 (1)	P(4)-C(34)	1.86 (1)

Angles around P Atoms			
Ni-P(1)-C(11)	120.2 (5)	Ni-P(3)-C(13)	118.4 (6)
Ni-P(1)-C(21)	113.8 (5)	Ni-P(3)-C(23)	117.6 (5)
Ni-P(1)-C(31)	114.8 (6)	Ni-P(3)-C(33)	115.5 (6)
C(11)-P(1)-C(21)	102.6 (7)	C(13)-P(3)-C(23)	98.7 (7)
C(11)-P(1)-C(31)	100.7 (7)	C(13)-P(3)-C(33)	102.4 (8)
C(21)-P(1)-C(31)	102.3 (7)	C(23)-P(3)-C(33)	101.5 (8)
Ni-P(2)-C(12)	113.0 (6)	Ni-P(4)-C(14)	123.5 (6)
Ni-P(2)-C(22)	120.3 (5)	Ni-P(4)-C(24)	122.1 (5)
Ni-P(2)-C(32)	114.2 (6)	Ni-P(4)-C(34)	107.6 (6)
C(12)-P(2)-C(22)	104.3 (7)	C(14)-P(4)-C(24)	97.2 (7)
C(12)-P(2)-C(32)	101.1 (7)	C(14)-P(4)-C(34)	100.9 (8)
C(22)-P(2)-C(32)	101.6 (7)	C(24)-P(4)-C(34)	101.9 (8)

BF_4^- Anion Distances							
B-F(1)	1.31 (2)	B-F(2)	1.34 (3)	B-F(3)	1.31 (4)	B-F(4)	1.36 (2)

BF_4^- Anion Angles					
F(1)-B-F(2)	110 (3)	F(1)-B-F(3)	114 (3)	F(1)-B-F(4)	108 (2)
F(2)-B-F(3)	113 (2)	F(2)-B-F(4)	102 (3)	F(3)-B-F(4)	107 (4)

[a] Data given in parentheses are the corresponding ones given for $[NiBr(P(OMe)_3)_4]BF_4$.[8]

Nickel–phosphorus distances ($Ni-P_{ax}$ = 2.247 (4) and 2.244 (4) Å; $Ni-P_{eq}$ = 2.290 (5) and 2.257 (5) Å) are larger than in the phosphite species by about 0.06 Å ($Ni-P_{ax}$ = 2.181 (2) and 2.180 (2) Å; $Ni-P_{eq}$ = 2.187 (2) and 2.239 (2) Å). In either compound, one equatorial nickel–phosphorus bond, Ni–P(3), is larger by about 0.05 Å than the three other which range over an interval 0.01-Å wide. In general, the nickel–phosphorus distances in $[NiBr(PMe_3)_4]^+$ are significantly larger than the ones observed in other trigonal-bipyramidal pentacoordinate nickel(II) compounds (Table IX) except for $Ni(CN)_2(PPh(OEt)_2)_3$ and $Ni(CN)_2(PPhMe_2)_3$ where one equatorial nickel-phosphorus bond was found to measure 2.289 (5) and 2.261 (3) Å, respectively.[17]

The nickel–bromine distance of 2.515 (2) Å is also larger than in the phosphite species (2.456 (1) Å). It is intermediate between the equatorial nickel bromine distances either of 2.451 (4) and 2.553 (4) Å or 2.426 (4) and 2.580 (4) Å reported for the trigonal bipyramid $NiBr_2(PMe_3)_3$.[3b]

Thus, comparison of the two structures shows, for $[NiBr(P(OMe)_3)_4]^+$, shorter nickel–phosphorus and nickel–bromine bonds and less distorted P–Ni–P or Br–Ni–P angles, a result which can be related not only to the smaller cone angle of $P(OMe)_3$ (107 ± 2°) compared with that of PMe_3 (118 ± 4°)[19] but also to the better ($\sigma + \pi$)-bonding character of the phosphite ligand compared to the essentially σ-bonding ability of PMe_3. This conclusion is in agreement with the experimental fact that an increase of the electronegativity of the phosphorus ligand makes it a better participant in π-back-bonding and shortens the nickel–phosphorus bond lengths (Table VIII). This is observed in cobalt(II) complexes, where the molecular C_{2v} trigonal-bipyramidal structures of $CoBr_2(PHPh_2)_3$ ($Co-P_{ax}$ = 2.20, 2.23 Å; $Co-P_{eq}$ = 2.18 Å) and $CoBr_2(PF_2Ph)_3$ ($Co-P_{ax}$ = 2.158 Å; $Co-P_{eq}$ = 2.12 Å) have been determined.

However, on the contrary to molecular trigonal-bipyramidal complexes $NiX_2(PR_3)_3$, in the cationic complexes $[NiX(PR_3)_4]^+$, the axial nickel–phosphorus bond lengths are smaller than the equatorial one. This result is in accord with the assumption of Hoffmann et al.[24] that in d^8 molecules, on the basis of repulsion pairs, when the d_{z^2} orbital is empty, the axial bond length will be shorter than the equatorial one. This was observed for $[Ni(P(OCH)_2(CH_2)_3)_5]^{2+}$ where $Ni-P_{ax}$ = 2.14 Å and $Ni-P_{eq}$ = 2.19 Å[25] but has not been observed, until now, for molecular complexes when two equatorial halides are present.

The role played by steric effects, although difficult to quantify, is important as shown by the general increase of the bond lengths when going from $NiBr_2(PMe_3)_3$ to $[NiBr(PMe_3)_4]^+$ (Table VIII).

The best least-squares plane which can be fitted to include the nickel atom and the equatorial atoms Br, P(3), and P(4) is

$$0.3993x - 0.9168y - 0.0064z = 1.8314$$

(Ni, 0.008 Å; Br, 0.002 Å; P(3), 0.003 Å; P(4), 0.003 Å) which shows that the nickel atom is in the equatorial plane. However, the angles around the nickel atom (P(3)–Ni–P(4) = 122.4 (2)°, P(3)–Ni–Br = 111.1 (1)°, and P(4)–Ni–Br = 126.6

Table IX. Axial and Equatorial Bond Lengths (Å) of Trigonal-Bipramidal Ni(II) and Co(II) MX_2L_3 and $[MXL_4]^+$, Complexes

compd	geometry[a]	Ni–P_{ax}	Ni–P_{eq}	Ni–X	ref
$NiI_2(PHPh_2)_3$	TBP cis-eq (C_{2v})	2.18 2.22	2.13	2.80 2.49	20
$NiI_2(P(OMe)_3)_3$	TBP cis-eq (C_{2v})	2.183 2.180	2.169	2.657 2.664	21
$[NiI(TEP)_2]I$	SPY		2.231; 2.239 2.218; 2.200	2.797	22
$NiBr_2(PMe_3)_3$	TBP cis-eq (C_{2v})	2.20 2.21 2.20 2.21	2.19 2.20	2.451 2.553 2.426 2.58	2
$Ni(CN)_2(PPhMe_2)_3$	TBP trans (D_{3h})		2.223 2.223 2.261	1.87 1.86	17
$Ni(CN)_2(PPh(OEt)_2)_3$	TBP trans (D_{3h})		2.189 2.205 2.289	1.87 1.89	17
$CoBr_2(PHPh_2)_3$	TBP cis-eq (C_{2v})	2.20 2.23	2.18	2.33 2.54	20
$CoBr_2(PF_2Ph)_3$	TBP cis-eq (C_{2v})	2.158 2.158	2.12	2.383 2.367	23
$[NiBr(P(OMe)_3)_4]^+$	TBP (C_{2v})	2.181 2.180	2.239 2.187	2.456	8
$[NiBr(PMe_3)_4]^+$	TBP (C_{2v})	2.247 2.244	2.29 2.257	2.515	this work

[a] TBP = trigonal bipyramid, SPY = square pyramid.

(2)°) are significantly different from 120°, but their sum is 360° within experimental range error.

As in the case of $[NiBr(P(OMe)_3)_4]^+$, $[NiBr(PMe_3)_4]^+$ also exhibits distortion from ideal trigonal-bipyramidal behavior, the axial ligands being forced toward the bromine atom. The angle P_{ax}–Ni–P_{ax} of 167.1 (2)° is slightly less opened toward 180° than observed in the phosphite species (172.3 (1)°). Nickel, bromine, and axial phosphorus atoms are practically coplanar: deviations from the best least-squares plane through these four atoms

$$0.1904x + 0.0801y + 0.9784z = 7.9368$$

are 0.03 Å for Ni, 0.004 Å for Br, and 0.02 Å for P(1) and P(2). This plane is closely perpendicular (90.3°) to the equatorial plane.

Axial phosphorus–bromine distances of 3.180 (4) Å and 3.182 (4) Å compare favorably with equivalent distances of 3.192 (2) and 3.154 (2) Å in $[NiBr(P(OMe)_3)_4]^+$ and are considerably shorter than the van der Waals distances (3.95 Å).[16] In $NiBr_2(PMe_3)_3$ close contacts between axial phosphorus and equatorial bromine atoms, ranging from 3.169 to 3.328 Å, were also observed.[3b] It is also worthwhile to notice that P_{ax}–P_{eq} distances range from 3.25 to 3.30 Å, which is dramatically shorter than the van der Waals P–P contact (3.8 Å). In contrast, the P_{eq}–P_{eq} distance of 3.98 Å is slightly larger than the van der Waals contact. Such a situation is not an exception since it is also observed in other pentacoordinate Ni(II) complexes with monodentate phosphorus ligands.[3b,8,21]

From the planarity of nickel, bromine, and axial phosphorus atoms and from the bending of the axial phosphorus atoms toward the bromine atom in $[NiBr(P(OMe)_3)_4]^+$, Verkade et al. concluded that "interestingly this crowding does not cause a distortion toward the tetragonal pyramid as in other nickel complexes".[8] The same can be said concerning $[NiBr(PMe_3)_4]^+$, at least as far as the distortion is expected to result from a Berry mechanism around the nickel–bromine axis. In order to settle quantitatively this conclusion, we have used Muetterties' pairing dihedral angle criteria.[27a] The ligands around the nickel atom are inequivalent, since two sets of significantly different Ni–ligand bond lengths are observed ($(Ni–P)_{av}$ = 2.26 Å and Ni–Br = 2.51 Å). We have thus used the dihedral-angle method extended to inequivalent ligand systems, as has been proposed by Kouba and Wreford.[27b] The

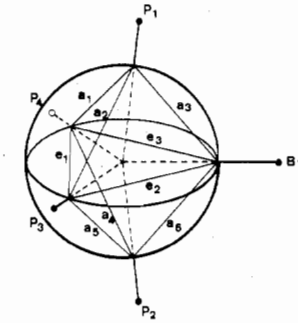

Figure 2. Projection of the ligands onto a sphere to form the inscribed polyhedron used to calculate the dihedral angles.

Table X. Dihedral Angles (deg) for $[NiBr(PMe_3)_4]BF_4$ and $[NiBr(P(OCH_3)_3)_4]BF_4$ Compared with the Equivalent Ones Calculated for Both Trigonal-Bipyramidal (TBP) and Square-Pyramidal (SPY) Ideal Geometries[a]

	ideal TBP	$[NiBr(P(CH_3)_3)_4]^+$	ideal SP	$[NiBr(P(OCH_3)_3)_4]^+$
$\delta(a_1)$	101.5	105.7	119.8	104.8[a]
$\delta(a_2)$	101.5	95.7	75.7	99.2
$\delta(a_3)$	101.5	103.3	119.8	100.6
$\delta(a_4)$	101.5	105.6	119.8	105.2
$\delta(a_5)$	101.5	96.2	75.7	98.3
$\delta(a_6)$	101.5	103.6	119.8	101.5
$\delta(e_1)$	53.1	61.8	75.7	56.3
$\delta(e_2)$	53.1	55.3	75.7	55.2
$\delta(e_3)$	53.1	42.0	0.0	47.6

[a] For the numbering system of edges, see Figure 2. [b] Calculated from structural data given in ref 8.

calculated dihedral angles shown in Table IX are related to the polyhedron built on points lying on the Ni–ligand bond lines and equidistant from the Ni atom (Figure 2). In Table IX, axial ($\delta(a_i)$'s) and equatorial ($\delta(e_i)$'s) calculated angles are compared with equivalent angles determined in both trigonal-bipyramidal and square-pyramidal (assuming the L_{eq}–M–L_{ax} angle to be 102°) idealized geometries.

If in the solid state, $[NiBr(PMe_3)_4]^+$ were lying on a Berry reaction path toward the square pyramid with Ni–Br as the fourfold or pseudofourfold axis, this should result in a pairing of dihedral angles $\delta(e_2)$ with $\delta(e_3)$ and $\delta(a_3)$ with $\delta(a_6)$ while $\delta(a_1)$, $\delta(a_2)$, $\delta(a_4)$, and $\delta(a_5)$ should be equivalent. This is not

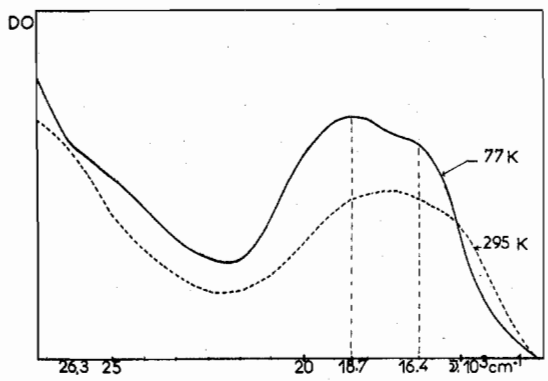

Figure 3. Temperature dependence of the solid-state (Nujol mull) electronic spectrum of $[NiBr(PMe_3)_4]BF_4$.

the case. Instead, inspection of Table X leads us to conclude that $\delta(a_2)$ (95.7°) pairs with $\delta(a_5)$ (96.2°), that $\delta(e_1)$ (61.8°) pairs with $\delta(e_2)$ (55.3°), and that $\delta(a_1)$ (105.7°), $\delta(a_3)$ (103.3°), $\delta(a_4)$ (105.6°), and $\delta(a_6)$ (103.6°) are nearly equivalent. Most interestingly, this way of pairing the dihedral angles is totally consistent with a Berry rearrangement mechanism toward a square-pyramidal configuration around Ni–P(3), which is precisely the largest nickel–phosphorus bond as outlined above. The same conclusion can be drawn from the examination of the dihedral angles in $[NiBr(P(OMe)_3)_4]^+$ (Table IX). This important feature will be discussed again later.

Bond lengths and angles of trimethylphosphine compare favorably with those reported for other structures. Ni–P–C angles range from 113.0 (6) to 123.5 (6)° against 110 (1)–121 (1)° in $NiBr_2(PMe_3)_3$[3b] and 114.8 (5)–118.3 (5)° in the Ni(I) compound $(Ni(PMe_3)_4)^+$;[28] C–P–C angles range from 97.2 (7) to 104.3 (7)° against 99 (1)–106 (1)° in $NiBr_2(PMe_3)_3$ and 100.2 (5)–102.8 (5)° in $[Ni(PMe_3)_4]^+$. Interestingly, C(11) and C(22) atoms respectively bound to apical P(1) and P(2) atoms are nearly coplanar with Ni Br, P(1), and P(2) atoms. Deviations from the best least-squares plane through these six atoms

$$0.2035x + 0.0963y + 0.9743z = 7.8694$$

are 0.055 Å for Ni, 0.019 Å for Br, 0.022 Å for P(1), 0.017 Å for P(2), 0.033 Å for C(11), and 0.007 Å for C(22). Therefore, the two axial $P(CH_3)_3$ groups have an eclipsed configuration with the carbon atoms as far as possible from the bromine atom, the result which confirms the presence of a "bonding" P–Br interaction.

The refinement of the BF_4^- anion has been possible within a fairly good accuracy. Its geometry fits well with the one derived by Verkade et al. in $[NiBr(P(OMe_3)_4]BF_4$. B–F distances range from 1.31 (2) to 1.36 (2) Å and F–B–F angles from 102 (3) to 114 (3)° (Table VII).

A.2. Solid-State Electronic Spectra. The 295 K solid-state electronic spectrum of $[NiBr(PMe_3)_4]BF_4$ (Figure 3) shows in the ligand field region the expected pattern of a d^8 low-spin trigonal bipyramid of C_{2v} symmetry. Lowering the temperature to 77 K improves the resolution of the spectrum where three ligand field transitions can be resolved at 16 400 cm^{-1} ($^1A_1 \rightarrow {}^1A_1$; $d_{x^2-y^2} \rightarrow d_{z^2}$), 18 700 cm^{-1} ($^1A_1 \rightarrow {}^1B_2$; $d_{xy} \rightarrow d_{z^2}$), and 26 300 cm^{-1} ($^1A_1 \rightarrow {}^1B_1$; $d_{xz} \rightarrow d_{z^2}$). Similar electronic spectra have been obtained for $[NiCl(PMe_3)_4]BF_4$ and $[NiI(PMe_3)_4]BF_4$.

B. Solution Study. B.1. Electronic Absorption Spectra. In dichloromethane, two major chemical processes can be detected by electronic spectroscopy:

$$[NiX(PMe_3)_4]BF_4 \rightleftharpoons [NiX(PMe_3)_3]BF_4 + PMe_3 \quad (A)$$

$$[NiX(PMe_3)_4]BF_4 \rightleftharpoons {}^1/_2NiX_2(PMe_3)_3 + {}^1/_2Ni(BF_4)_2 + {}^5/_2PMe_3 \quad (B)$$

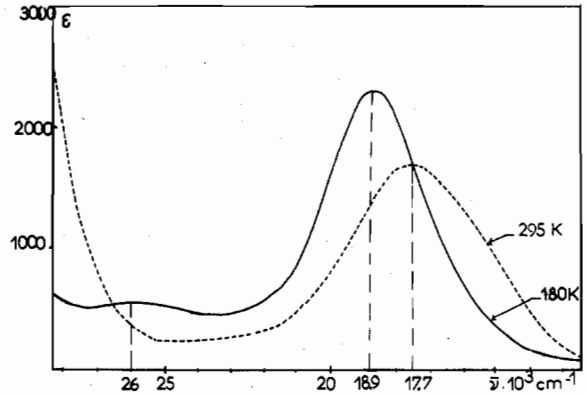

Figure 4. Temperature dependence of the electronic spectrum of $[NiCl(PMe_3)_4]BF_4$ (10^{-2} M) in dichloromethane containing excess PMe_3 (10^{-2} M/L) (PMe_3(total)/Ni molar ratio = 5).

This is expected since it is well-known that the pentacoordinate Ni(II) or Co(II) complexes with monodentate tertiary phosphine ligands are dissociatively unstable.[3a]

For X = Cl, reaction A is predominant. The electronic spectrum shows a shift of the ligand field band maximum toward the higher energies when the excess of PMe_3 is lowered (see Table VI) due to the increase of the concentration of the tetracoordinate square-planar species, characterized by a higher energy ligand field transition.[7] For X = I, reaction B is favored since without excess of PMe_3 the ligand field bands of $NiI_2(PMe_3)_3$ are present (at 13 700 and 16 300 cm^{-1} [3b]) and white crystals of $Ni(BF_4)_2$ precipitate from the dichloromethane solution. For X = Br, both reactions are operating.

At low temperature (180 K), the pentacoordinate cationic species $[NiX(PMe_3)_4]BF_4$ is stabilized. In accord with the law of mass action, this species is favored at high concentrations by adding excess PMe_3. Low-temperature $^{31}P\{^1H\}$ NMR shows that in 10^{-2} M $[NiX(PMe_3)_4]BF_4$ with 10^{-2} M excess PMe_3 solution, there is only one species present, and thus all of the elctronic spectra were recorded on 10^{-2}–2×10^{-2} M solutions in complexes.

The electronic spectrum of $[NiBr(PMe_3)_4]BF_4$, at 295 K, with 10^{-2} excess PMe_3, consists of a broad asymmetric ligand field band at about 18 250 cm^{-1} (Figure 4). This band can be deconvoluted, by Gaussian analysis, into two transitions at about 15 900 and 18 400 cm^{-1}, showing that the C_{2v} trigonal-bipyramidal geometry is preserved in solution. A small shoulder is present at about 14 600 cm^{-1}, in the absence of excess PMe_3, on the low-energy side of the ligand field band. This shoulder can be related to the presence of $NiBr_2(PMe_3)_3$ since its proportion increases at the expense of $[NiBr(PMe_3)_4]^+$, as the complex concentration is lowered by reaction B. The maximum of the ligand field band increases in intensity in the presence of excess PMe_3 (PMe_3 total/Ni molar ratio = 4, 5, and 10; Table VI). On lowering the temperature of the solution, one can observe (i) a small shift of the band maximum toward the higher energies (18 700 cm^{-1}), (ii) an increase of the extinction coefficient of the band maximum, indicating that the formation of the pentacoordinate cationic species is favored at low temperature, (iii) an increase of the symmetry of the ligand field band, in the order I > Br > Cl, and (iv) the resolution of a high-energy, less intense transition at 26 300 cm^{-1} for X = Cl and Br. This intensity pattern is similar to those observed for a large number of trigonal-bipyramidal low-spin Ni(II) complexes of both C_{3v} and D_{3h} symmetries[30] but was not expected for a C_{2v} molecule.

For $[NiCl(PMe_3)_4]BF_4$ solutions, no major differences are observed between the 295 and 180 K spectra (Figure 5). At 180 K, a broad asymmetric band at 18 900 cm^{-1} can be resolved, by Gaussian analysis, into two ligand field bands at 16 300 and 18 800 cm^{-1} (16 700 and 18 900 cm^{-1} in the sol-

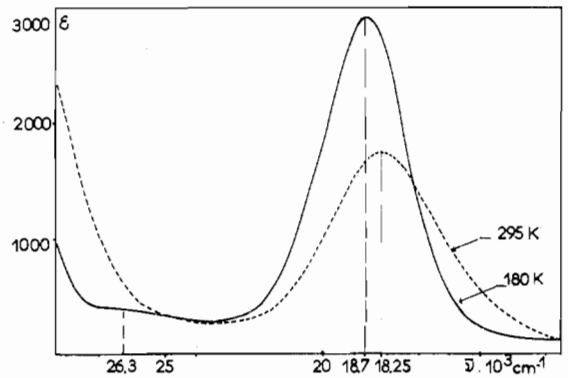

Figure 5. Temperature dependence of the electronic spectrum of $[NiBr(PMe_3)_4]BF_4$ (10^{-2} M) in dichloromethane containing excess PMe_3 (10^{-2} M/L) (PMe_3(total)/Ni molar ratio = 5).

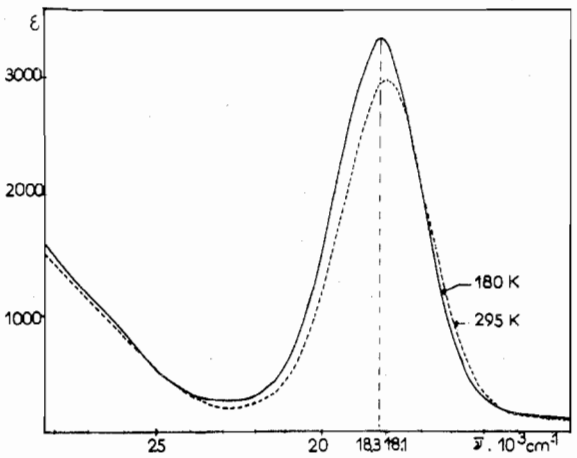

Figure 6. Temperature dependence of the electronic spectrum of $[NiI(PMe_3)_4]BF_4$ (10^{-2} M) in dichloromethane containing excess PMe_3 (10^{-2} M/L) (PMe_3(total)/Ni molar ratio = 5).

id-state spectrum), thus indicating the presence of the C_{2v} cationic isomer in solution. By adding excess PMe_3 and/or lowering the temperature, the same behavior as for $[NiBr(PMe_3)_4]BF_4$ is observed.

For $[NiI(PMe_3)_4]BF_4$ solutions, there is hardly any difference between the 295 and 180 K spectra (Figure 6). There is only one nearly symmetrical ligand field transition at about 18 100 cm^{-1}, in the presence or not of PMe_3 in excess, but the general behavior of the spectra is similar to that observed for X = Cl and Br. However, as we have seen before, in the absence of excess PMe_3, the molecular $NiI_2(PMe_3)_3$ species is present in solution, due to reaction B.

B.2. $^{31}P\{^1H\}$ Nuclear Magnetic Spectra. The three complexes are stereochemically nonrigid at room temperature, a result which was expected for a d^8 $[NiXL_4]^+$ pentacoordinate molecule.[10] However, the phosphorus exchange can be slowed down by lowering the temperature, and a resolved spectrum is obtained at 153 K for X = I and Br in CH_2Cl_2–CD_2Cl_2 and at 115 K for X = Cl in $CHClF_2$. It consists, for the three complexes, of two resolved triplets, characteristic of an A_2B_2 pattern (Figure 7). Thus, at low temperature, the three $[NiX(PMe_3)_4]BF_4$ complexes exhibit in solution the same trigonal-bipyramidal geometry with X equatorial, as was found in the solid state. At the concentrations used—10^{-2} M in complexes and 10^{-2} M excess PMe_3—no other species were observed.

The NMR parameters are reported on Table VII. By comparison with the molecular $NiX_2(PMe_3)_3$[9,18] and cationic $[Ni(PMe_3)_5]^{2+}$ [18] species, and as observed by Meakin and Jesson[26] in cationic d^8 $[ML_5]^{n+}$ species, the phosphorus resonance with the largest downfield chemical shift can be assigned to the axial phosphine ligand. The chemical shifts observed for the equatorial phosphines are similar (about −29 ppm) for the three complexes, indicating only small interactions of the halide with the two equatorial phosphines. On the other hand, stronger interactions are present between the two axial phosphines and the halide since the chemical shift depends strongly on the halide: δ_{Cl} = 1.00 ppm, δ_{Br} = −1.8 ppm, δ_I = −5.0 ppm.

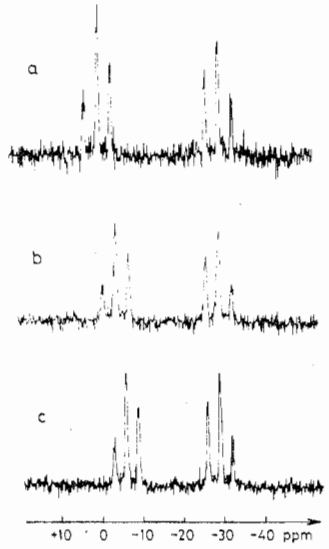

Figure 7. $^{31}P\{^1H\}$ FT NMR spectra at 24.28 MHz of 2×10^{-2} M solutions of (a) $[NiCl(PMe_3)_4]BF_4$, (b) $[NiBr(PMe_3)_4]BF_4$, and (c) $[NiI(PMe_3)_4]BF_4$ in $CHClF_2$ at −120 °C, with excess PMe_3 (2×10^{-2} M/L).

By increasing the temperature of a 2×10^{-2} M $CHClF_2$ solution of $[NiCl(PMe_3)_4]BF_4$ containing PMe_3 in excess (2×10^{-1} M) from 115 to 180 K, one observes the broadening of the two resolved triplets which coalesce into a single line. This behavior indicates that intramolecular phosphine exchange occurs. Above 180 K, the singlets of the free phosphine and the complex begin to broaden and coalesce into a single line indicating an intermolecular exchange process. This process has not been investigated. One sees that, as observed in other Ni(II) complexes,[5] the intramolecular exchange begins at lower temperature than the intermolecular one and can thus be studied independently. From 115 to 180 K, the peak of PMe_3 in excess remains sharp. Variable excesses of PMe_3 (complex to free ligand ratio varying from 1:1 to 1:20) did not affect the rate of the intramolecular exchange process between 115 and 180 K. For X = Br and I, the intramolecular exchange begins at higher temperature (153 K in $CHClF_2$). For this reason, the free energies of activation ΔG^* (kcal/mol) were measured at 169 K: 6.6 ± 0.2 for X = Cl, 7.8 ± 0.2 for X = Br, and 8.2 ± 0.2 for X = I.

IV. Discussion

The crystal structure presented here shows that the cation $[NiBr(PMe_3)_4]^+$ has a geometry which is a somewhat distorted version of a trigonal bipyramid of C_{2v} symmetry, similar to that of $[NiBr(P(OMe)_3)_4]^+$, a result which indicates that (i) the trigonal bipyramid is the perferred geometry in the ground state for a low-spin d^8 pentacoordinate Ni(II) complex with a monodentate sterically unhindered phosphine ligand and (ii) the halide prefers the equatorial site of the trigonal bipyramid.

Two conclusions can be deduced from the distortion observed in the crystalline state:

(1) The presence of interactions is apparent between the two axial phosphorus atoms and the three equatorial atoms Br and P(3) and P(4), since the P_{ax}–P_{eq} distances of 3.25–3.35 Å and P_{ax}–Br distances of 3.18 Å are considerably shorter than the van der Waals distances of respectively 3.8 and 3.95 Å. The

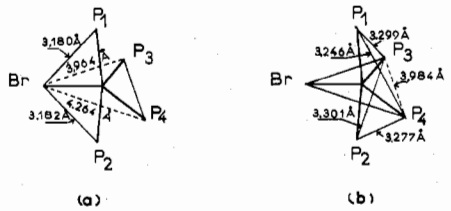

Figure 8. Illustration of the differences (a) in P–Br distances and (b) in P–P distances in $[NiBr(PMe_3)_4]BF_4$.

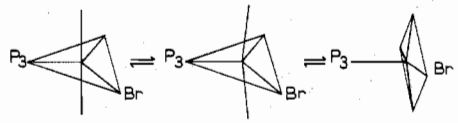

Figure 9. Geometric reaction path for conversion of the trigonal bipyramid to the square pyramid in the C_{2v} $[NiX(PMe_3)_4]^+$ cation (with Ni–P(3) as pivot).

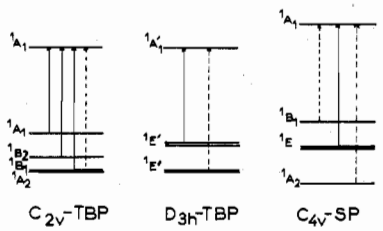

Figure 10. Effect of the geometry and site symmetry on the ligand field levels of $[NiX(PMe_3)_4]^+$ complexes. Orbitally allowed (—) and forbidden (---) transitions are shown (TBP = trigonal bipyramid, SP = square pyramid).

presence of a P_{ax}–Br interaction is suggested too since the two axial PMe_3 groups have an eclipsed configuration with the carbon atoms as far as possible from the bromine atom. This kind of interaction is present too in $[NiBr(P(OMe)_3)_4]BF_4$, $NiBr_2(PMe_3)_3$, and $NiI_2(P(OMe)_3)_3$, that is, when the halides are in the equatorial position of the trigonal bipyramid (Figure 8).

(2) The second distortion has been determined by using Muetterties' pairing dihedral angles criteria,[27] which is much more effective to determine the position of the molecule on the geometrical reaction path between a regular trigonal bipyramid and a regular square pyramid than the geometrical coordinates around Ni. Thus we have been able to show that, in the solid state, the molecule is on the geometric reaction path toward a square-pyramidal configuration with the longest $Ni–P(3)_{eq}$ bond as pivot but is on the trigonal-bipyramidal side (Figure 9).

The solid-state electronic spectra of $[NiX(PMe_3)_4]BF_4$ with three resolved ligand field transitions can thus be assigned to the C_{2v} symmetry and the assignments are in good agreement with the one reported for other C_{2v} trigonal-bipyramidal Ni(II) low-spin complexes[3b] (Figure 10).

However, when these complexes are dissolved in dichloromethane with PMe_3 in excess to prevent dissociation, the electronic spectra at room temperature show one asymmetric ligand field band. When X = Cl and Br, a less intense transition can be resolved on the low-energy side, showing that the stereochemistry is retained in solution. At low temperature, the intensity and the symmetry of the ligand field band increase and a less intense transition on the higher energy side can be resolved for X = Cl and Br. The low-temperature behavior (180 K) could suggest a D_{3h} or a C_{3v} isomer,[30] but the $^{31}P\{^1H\}$ NMR spectra of the same solutions at low temperature show only the two triplets characteristic of the C_{2v} isomer and not the doublet and quartet expected for the other two geometries.[6,18] Moreover, the presence of a square pyramid with X axial (C_{4v}) which would also accommodate

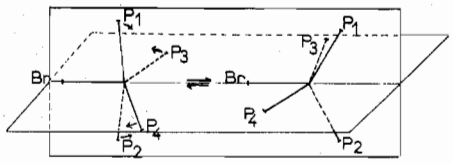

Figure 11. Berry mechanism: reaction path for intramolecular rearrangement. The two axial P(1) and P(2) ligands exchange positions with the two equatorial P(3) and P(4) ligands in a single step (Ni–Br as pivot).

a symmetrical one-transition ligand field spectrum (Figure 10) can be ruled out since the ligand field transitions would then occur at higher energies, for example, 20 160 cm^{-1} (ϵ 1560) in $[NiBr(VPP)]^+$[29] (VPP = *cis*-1,2-bis(diphenylphosphino)ethylene), 20 600 cm^{-1} (ϵ 2600) in $[NiI(TEP)_2]^+$[22] (TEP = tris(triethylphosphino)ethane). To our knowledge, no square-pyramidal low-spin Ni(II) complexes have been reported when halide and monodentate tertiary phosphine ligands are present.

The presence of the C_{2v} isomer is also confirmed in solution since the position of the ligand field band is not very dependent on the anionic ligand X. The values are, at 180 K, 18 900 cm^{-1} (ϵ 2400) for X = Cl, 18 700 cm^{-1} (ϵ 2900) for X = Br, and 18 300 cm^{-1} (ϵ 3300) for X = I^-, when $PMe_3(total)/Ni = 5$. On the contrary, the ligand field transitions are halide dependent in C_{3v} trigonal-bipyramidal complexes.[30]

Thus, since the molecules belong to the C_{2v} point group, all of the ground and excited states are expected to be nondegenerate, and no dynamic Jahn–Teller effect operates. There are only small changes in the shape of the ligand field bands in the solid-state spectra after cooling from 295 to 77 K. Thus the symmetrical ligand field spectra of $[NiX(PMe_3)_4]BF_4$, in dichloromethane at 180 K, may be related (i) to temperature-dependent vibronic interactions which decrease when the temperature is lowered or (ii) to the presence of a nearly symmetric ligand field in the equatorial plane resulting from the P_2X donor set (in the order P_2I more symmetrical than P_2Br than P_2Cl). Consequently, the complexes may have around the nickel atom a D_{3h} rather than a C_{2v} local symmetry. This result agrees well with the fact that a very similar ligand field spectrum is obtained for TBP $[Ni(PMe_3)_5](BF_4)_2$:[18] one ligand field band at 18 850 cm^{-1} at 180 K in dichloromethane. However, it is difficult to know if this pseudo-D_{3h} symmetry around the Ni atom may or may not be related to the presence of P_{ax}–X and P_{ax}–P_{eq} interactions in the TBP.

As expected[10] for pentacoordinate Ni(II) (NiL_5 or NiL_4L'), the $[NiX(PMe_3)_4]^+$ complexes are stereochemically nonrigid at room temperature. However, the rate of the exchange process can be reduced to a frequency that is low on the NMR time scale at low temperature (163–113 K). The simplest process to explain the intramolecular phosphorus exchange in C_{2v} $[NiXL_4]^+$ complexes is the Berry pseudorotation (Figure 11). This process is expected to have a very low energy barrier (as low as for $[NiL_5]^{2+}$) since the transition state or the reaction intermediate may still have the C_{4v} square-pyramidal geometry with the unique X ligand at the axial site. The free energy of activation for the intramolecular rearrangement in $[Ni(PMe_3)_5](BF_4)_2$ is 6.2 ± 0.2 kcal mol^{-1} at 130 K.[18] In the $[NiX(PMe_3)_4](BF_4)$ complexes, the barriers are also low, supporting a Berry exchange mechanism, but increase significantly in the order Cl < Br < I.

In the absence of a π-back-bonding argument, as was reported in the $Fe(CO)_{5-n}L_n$ compounds,[30,31] the increase in barrier may be reasonably attributed to the encumbering of the rearrangement path due to the presence of an P_{ax}–X interaction, which has been noted in the solid-state structure of the bromine complex and seemed to persist in solution. Such an explanation has been proposed to explain the presence of

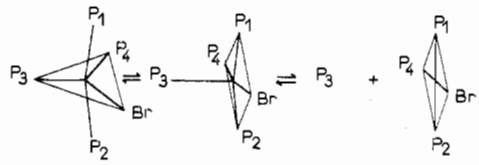

Figure 12. Reaction path for ligand (P(3)) dissociation (intermolecular rearrangement process).

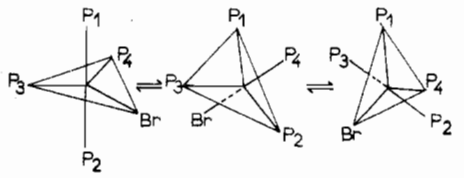

Figure 13. Double Berry mechanism: reaction path for intramolecular rearrangement with Ni–P(3) as the first pivot and Ni–P(1) as the second one.

a rearrangement barrier higher than 15 kcal/mol for NH_2PF_4.[33]

However, if we remember that the solid-state structure is a trigonal bipyramid distorted toward a square pyramid along the $Ni–P(3)_{eq}$ bond, two other reaction paths may be envisaged to explain the phosphine exchange.

The first one can be described as a dissociative reaction along this $Ni–P(3)_{eq}$ bond (Figure 12), involving a simultaneous intramolecular rearrangement and intermolecular ligand exchange. However, since the shape of the variable-temperature $^{31}P\{^1H\}$ NMR spectra of the complexes are not affected by a variable excess of PMe_3, this process can be ruled out.

The second one can be described by a double Berry process (Figure 13) with the $Ni–P(3)_{eq}$ bond as a first pivot. However, the low-temperature $^{31}P\{^1H\}$ NMR spectra of solutions of the complexes show only one signal for the two equatorial phosphines, indicating (i) that in solution the two $Ni–P_{eq}$ bonds are equivalent or (ii) that the isomerization of the two bonds is very rapid. Consequently, the Ni–P(3) bond has lost its special character. Moreover, such a double Berry process, which implies an axial halide in the intermediate state, is unfavored as, until now, no pentacoordinate Ni(II) complexes with PMe_3 and/or $P(OMe)_3$ ligands having halide as axial ligands have been reported. We suggest, therefore, that the axial–equatorial PMe_3 exchange is an intramolecular process occurring through a single Berry mechanism with the halide as pivot.

However, the presence of a dissociative reaction path along the $Ni–P(3)_{eq}$ pivot—a more energetic path than the Berry process—showing that in this molecule an equatorial phosphine ligand ought to be easily substituted is very promising and will be discussed in more detail in a following paper.[18]

Acknowledgment. We thank Mr. A. Mari for the preparation of the trimethylphosphine and the determination of the magnetic susceptibilities. This work has been technically supported in part (X-ray structure determination) by the Centre National de la Recherche scientifique, the Délégation Générale à la Recherche Scientifique et Technique, and the Direction de l'Enseignement Supérieur et de la Recherche. The generous support of the Swiss National Science Foundation is acknowledged through grant No. 2 291-0.77.

Registry No. $[NiBr(PMe_3)_4]BF_4$, 67889-86-5; $[NiCl(PMe_3)_4]BF_4$, 67889-84-3; $[NiI(PMe_3)_4]BF_4$, 67889-82-1.

Supplementary Material Available: A listing of calculated and observed structure factors (Table III) (12 pages). Ordering information is given on any current masthead page.

References and Notes

(1) Presented in part at the 4th European Crystallographic Meeting, Oxford; Abstract No. PII, 142. Abstracted, in part, from the Ph.D. Thesis of Pierre F. Meier, Université de Lausanne, 1978.
(2) (a) Laboratoire de Chimie de Coordination du CNRS. (b) Institut de Chimie Minérale et Analytique.
(3) (a) R. Morassi, I. Bertini, and L. Sacconi, *Coord. Chem. Rev.*, **11**, 343 (1973). (b) J. W. Dawson, T. J. McLennan, W. Robinson, A. Merle, M. Dartiguenave, Y. Dartiguenave, and H. B. Gray, *J. Am. Chem. Soc.*, **96**, 4428 (1974). (c) E. J. Lukosius and K. J. Coskran, *Inorg. Chem.*, **14**, 1922 (1975).
(4) M. F. Ludmann, M. Dartiguenave, and Y. Dartiguenave, *Inorg. Chem.*, **16**, 440 (1977), and references therein.
(5) A. D. English, P. Meakin, and J. P. Jesson, *J. Am. Chem. Soc.*, **98**, 422 (1976).
(6) H. F. Klein, H. H. Karsch, and W. Buchner, *Chem. Ber.*, **107**, 537 (1974).
(7) P. Rigo and M. Bressan, *Inorg. Chem.*, **11**, 1314 (1972).
(8) O. S. Milbrath, J. P. Springer, J. C. Clardy, and J. G. Verkade, *Inorg. Chem.*, **14**, 2665 (1975).
(9) P. Meier, A. Merbach, M. Dartiguenave, and Y. Dartiguenave, *J. Am. Chem. Soc.*, **98**, 6402 (1976).
(10) J. P. Jesson and E. L. Muetterties in "Dynamic Nuclear Magnetic Resonance Spectroscopy", L. M. Jackman and F. A. Cotton, Eds., Academic Press, New York, N.Y., 1975, p 270.
(11) W. Wolfsberger and H. Schmidbaur, *Synth. Inorg. Met.-Org. Chem.*, **4**, 149 (1974).
(12) G. Foex, "Constantes Sélectionnées—Diamagnétisme et Paramagnétisme", Masson, Paris, 1957.
(13) C. Ammann, P. Meier, and A. E. Merbach, submitted for publication.
(14) In addition to local programs for the C11-IRIS 80, local modifications of the following programs were employed: Germain, Main, and Woolfson's MULTAN program, Zalkin's FORDAP Fourier program, Ibers and Doedens' NUCLS least-squares program, Busing and Levy's ORFLS program, and Johnson's ORTEP II thermal plotting program.
(15) D. T. Cromer and J. T. Waber, "International Tables for X-ray Crystallography", Vol. IV, Kynoch Press, Birmingham England, 1965, Table 2.2A; D. T. Cromer, *ibid.*, Table 2-3.
(16) L. Pauling, "The Nature of the Chemical Bond", 3rd ed., Cornell University Press, Ithaca, N.Y., 1960.
(17) J. K. Stalick and J. A. Ibers, *Inorg. Chem.*, **8**, 1084, 1089 (1969).
(18) P. Meier, A. Merbach, M. Dartiguenave, and Y. Dartiguenave, to be submitted for publication.
(19) C. A. Tolman, *J. Am. Chem. Soc.*, **92**, 2956 (1970).
(20) J. A. Bertrand and D. L. Plymale, *Inorg. Chem.*, **5**, 879 (1966).
(21) L. J. Vande Griend, J. C. Clardy, and J. G. Verkade, *Inorg. Chem.*, **14**, 711 (1975).
(22) E. C. Alyea and D. W. Meek, *Inorg. Chem.*, **11**, 1029 (1972).
(23) O. Stelzer, W. S. Sheldrick, and J. Subramanian, *J. Chem. Soc., Dalton Trans.*, 966 (1977).
(24) A. R. Rossi and R. Hoffmann, *Inorg. Chem.*, **14**, 365 (1975).
(25) E. F. Riedel and R. A. Jacobson, *Inorg. Chim. Acta*, **4**, 407 (1970).
(26) P. Meakin and J. P. Jesson, *J. Am. Chem. Soc.*, **96**, 5751 (1974).
(27) (a) E. L. Muetterties and L. J. Guggenberger, *J. Am. Chem. Soc.*, **96**, 1748 (1974); (b) J. K. Kouba and S. S. Wreford, *Inorg. Chem.*, **15**, 1463 (1976).
(28) A. Gleizes, M. Dartiguenave, Y. Dartiguenave, J. Galy, and H. F. Klein, *J. Am. Chem. Soc.*, **99**, 5187 (1977).
(29) C. A. McAuliffe and D. W. Meek, *Inorg. Chem.*, **8**, 904 (1969).
(30) J. W. Dawson, H. B. Gray, J. E. Hix, J. R. Preer, and L. M. Venanzi, *J. Am. Chem. Soc.*, **94**, 2979 (1972).
(31) S. T. Wilson, N. J. Coville, J. R. Shapley, and J. A. Osborn, *J. Am. Chem. Soc.*, **96**, 4038 (1974).
(32) L. Kruczynski, L. K. K. Lishing Man, and J. Takats, *J. Am. Chem. Soc.*, **96**, 4006 (1974).
(33) A. W. Cowley and J. R. Schweiger, *J. Chem. Soc., Chem. Commun.*, 560 (1972).